# Transient Thermal Stress Calculation of a Shell and Tube Condenser with Fixed Tubesheet

Marek Pernica[1], Tomáš Létal[1], Pavel Lošák[1], Martin Nad̆[1], Marcus Reppich[2,*], and Zdeněk Jegla[1]

**DOI:** 10.1002/cite.202100036



The present article deals with transient thermal stress calculation on a safety horizontal shell and tube condenser. This condenser is used in a power plant for cooling of hot steam diverted from the turbine in the case of its emergency shutdown. The standard stress calculation was provided according to the EN 13445 standard in steady regime. As consistent with this calculation, an expansion joint must be used on the shell. The main aim of this article is to describe a detailed calculation of the transient temperature field on the shell and tubes, using finite element method analysis, and longitudinal thermal stresses on the shell and tubes during the start-up process. Transient analyses are useable for more accurate EN 13445 calculation and, furthermore, for fatigue calculation.

**Keywords:** Condensers, Expansion joints, Transient temperature fields, Transient thermal stresses

*Received:* April 20, 2021; *revised:* May 27, 2021; *accepted:* July 02, 2021

## 1 Introduction

This article is focused on the transient calculation of longitudinal thermal stress, which arises on the shell and tube bundle during the start-up process of a shell and tube condenser with condensation in the shell side. Shell and tube condensers with shell side condensation are widely used in various industries, mainly in energy, food, or process industry. The condensing medium is fed to the shell. While it flows across the tube bundle, it is condensed on the outer surface of tubes cooled by a cooling medium. The condensate flows to the bottom of the shell and flows out from the condenser.

Calculation of stresses in the shell and tubes of a condenser is a complex problem. Three types of loads are expected: temperature, pressure, and exterior load. In this article, the temperature load during the start-up process is studied. To solve the temperature field, the estimate of the heat transfer coefficient is crucial. However, the condensation heat transfer coefficient is complicated to solve, especially on the condenser shell side. The first study focused on the condensation heat transfer coefficient on a single, smooth horizontal tube and was developed by Nusselt [1]. The improved Nusselt model was presented by Kern [2], who studied the condensing coefficient for different common tube bundle layouts. Many other authors presented their studies and models evaluating the condensation heat transfer coefficient. Honda et al. [3] tested different tube configurations of tube bundle with pure liquids as well as with mixtures. He found that the used liquid and its mix composition has great impact on the condensation heat transfer coefficient. Many other studies evaluating the condensation heat transfer coefficient were presented in the past, e.g., by Cavallini et al. [4], Fuji and Oda [5]. Further models are published in condensation reviews [6, 7].

Computational fluid dynamics (CFD) is very up-to-date and is increasingly used for flow stream analysis of shell and tube heat exchangers. It provides detailed results of flow field including the condensation heat transfer coefficient. Karlsson and Vamling [8] presented the 2D CFD analysis executed on a shell and tube condenser with shell side condensation. Karlsson presented a vapor flow field calculation and condensation rate on a simplified model; he mentioned that the CFD analysis of condensation is a very complex process, which usually requires some simplifications due to the calculation time and convergence obtained for the solution. Many other simplifications are used in CFD studies. In [9], Wang et al. presented a shell and tube heat exchanger optimalization of shell flow. They neglected the thickness of baffles and the space between the baffles and the shell/tubes to reduce the computational time.

[1]Marek Pernica, Dr.-Ing. Tomáš Létal, Dr.-Ing. Pavel Lošák, Dr.-Ing. Martin Nad̆, Prof. Dr.-Ing. Zdeněk Jegla
Brno University of Technology, Institute of Process Engineering, Technická 2896/2, 616 69 Brno, Czech Republic.

[2]Dr.-Ing. Marcus Reppich
marcus.reppich@hs-augsburg.de
Augsburg University of Applied Sciences, Faculty of Mechanical and Process Engineering, An der Hochschule 1, 86161 Augsburg, Germany.

The transient temperature field is needed for the thermal stress calculation during the start-up process. In [10], an overview is presented of developed dynamic models for vapor compression systems. Another mathematical model is presented by Llopis et al. [11]. In this study, the validation with experimental data was provided with satisfactorily small errors. Transient numerical modeling of a multi-pass shell and tube heat exchanger based on the finite-volume method is presented in [12]. Fritz et al. [12] validated the results from the model with theoretical as well as experimental data from available literature. They used a simplified 1D fluid flow model according to the cell method [13, 14], which is a special type of finite element method. They pointed out that this model is a good tradeoff between accuracy and speed of the simulation.

In industry, commercial software for thermal-hydraulic rating is commonly used, e.g., HTRI [15], CHEMCAD [16], and ASPEN [17]. They are based on semiempirical models, allowing relatively easy and fast thermal-hydraulic rating of heat exchangers. CHEMCAD [16] is able to calculate a wide range of process industry equipment, but it does not allow to calculate the thermal-hydraulic heat exchanger rating in great detail. With the HTRI [15] in module Xist, which is a designation for heat exchanger thermal-hydraulic rating, it is not possible to calculate the transient behavior of heat exchangers.

The review above shows that a lot of research has been done on thermal-hydraulic rating of condensers. It is possible to use a broad range of mathematical condensation models as well as modern CFD methods or commercial software for thermal-hydraulic rating of condensers.

The transient model for monitoring the thermal stresses in pressure components of a steam power boiler is presented in [18]. Taler et al. showed two methods of transient thermal stress calculation. The first method was based on the measurement of unsteady temperature on the outer surface of the pressure component and the second one used FEM analysis. In [19], the start-up process of the heat recovery steam generator (HRSG) unit is investigated. Kim et al. developed a program for characteristic prediction of the HRSG. They used it for simulation of the HRSG start-up and investigated maximal thermal stresses. They confronted the thermal stresses during the start-up process with the maximal allowable limit of material. In [20], Taler et al. presented a seminumerical time-dependent method to determine thermal stresses in pressurized thick-walled elements of steam boilers. The review of literature on transient thermal stresses shows that the start-up and shut-down issue is mainly observed on the parts of steam boilers. However, in the case of this article, a transient thermal stress calculation can be also used for condensers. The thermal stress between the shell and tubes cannot be neglected. It should cause cracks on the shell, tubes, or joints of tubes with the tube sheet.

A horizontal condenser with condensation on the shell side is investigated in this article. This condenser is a countercurrent flow type, and it is used as a safety condenser for turbine steam condensation. The condenser shell length is 2024 mm, the outer shell diameter is 355.6 mm, and it has 137 tubes with an outer diameter of 16 mm and a wall thickness of 1 mm. Three segmental baffles are used in the shell. In the limit working state, the steam inlet temperature is 360 °C and cooling water with a temperature of 20 °C flows to the tubes. In this state, the expansion joint on the shell is needed according to the EN 13445 [21] standard calculation. Therefore, the main aim of this article is to investigate the start-up process and calculate the longitudinal stresses which can be indicated during the start-up. Moreover, this type of analyses could be used for more detailed thermal stress and fatigue calculation of heat exchangers. The shell expansion joint is a very expensive component susceptible to fatigue. The stresses in the presented case were estimated using a combination of methods. The commercial software HTRI was used for calculation of the heat transfer coefficient, FEM analyses were used for transient calculation of the wall temperature field, and in-house calculation was applied to solve the thermal stresses on the shell and tube bundle. Obviously, some simplifications were necessary as described below.

## 2 Methods

### 2.1 Temperature Field of Steam and Cooling Water

The commercial software HTRI was used primarily for estimation of heat transfer coefficient on the shell/tube side. This calculation was carried out for steady-state mode because, as mentioned earlier, HTRI is not able to calculate the thermal-hydraulic rating in the transient regime. The results of the heat transfer coefficient were used in the next part where the transient temperature field is described. The cooling water and hot steam were used as process media from HTRI media library. The inlet temperature of hot steam was set at 360 °C, pressure at 96 kPa, and its mass flow rate was set at 0.025 kg $s^{-1}$. The cooling medium in the tubes was water with an inlet temperature of 20 °C and a mass flow rate of 29.3 kg $s^{-1}$.

HTRI allows only for calculations of TEMA type [22] heat exchangers, but the investigated condenser is not the standard TEMA type. It has a reservoir for condensate in the middle of the shell length (Fig. 1). Therefore, a modified condenser model was used. The condensate reservoir was replaced by a standard outlet nozzle and moved towards the end of the shell (Fig. 2).

The results have shown that the vapor is completely condensed at a length coordinate of 500 mm from the steam inlet nozzle, which is approximately the position of the condensate reservoir. This should significantly affect the resulting heat transfer coefficient. The heat transfer coefficients inside the area of shell and tubes within the effective tube length are shown in Fig. 3. The heat transfer coefficient of

  

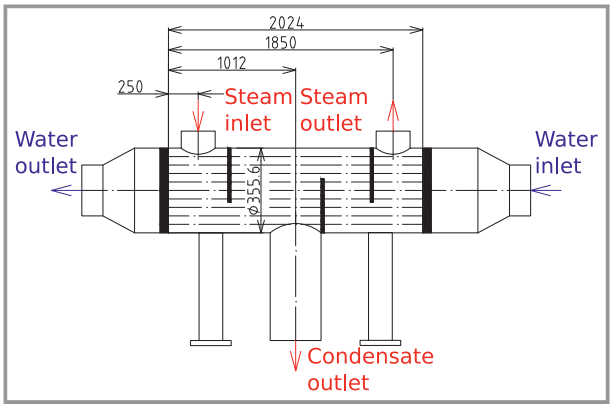


**Figure 1.** Investigated condenser scheme.

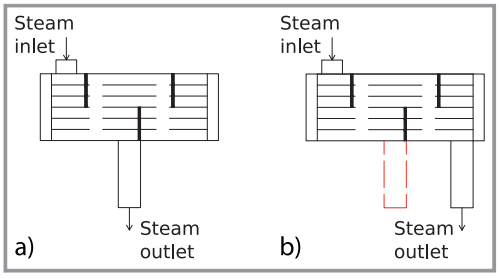


**Figure 2.** Change of position of condensate reservoir for HTRI calculation, a) real configuration, b) configuration for HTRI.

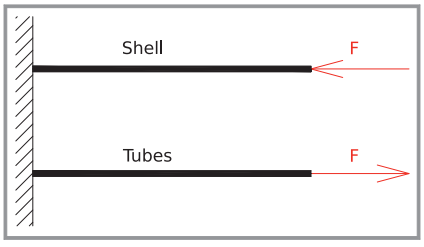


**Figure 3.** Heat transfer coefficient relative to length of shell/tube.

the tube side (line with square marker) is almost constant across the entire effective length of the tubes. However, the heat transfer coefficient on the shell side (line with circle marker) highly increases in the stream inlet area relative to the length, where almost all the vapor condenses. Then, the heat transfer coefficient on the shell side rapidly decreases. In the steam outlet area, the heat transfer coefficient on the shell side is only around 984 $W\,m^{-2}K^{-1}$.

## 2.2 Transient FEM Analyses

The second step is the calculation of the transient temperature field of the investigated condenser during the start-up process. The transient thermal FEM analyses were used for temperature field evaluation on the shell and tube condenser over time. For this simulation, ANSYS Mechanical R2 2019 [23] was used. For the initial condition, a uniform temperature of 20 °C and a heat transfer coefficient of air of 20 $W\,m^{-2}K^{-1}$ were used. These values represent a state before the start-up process. As the time and boundary condition of the first time step, the bulk temperature field and heat transfer coefficient from the steady state of HTRI calculation and the time of the stream passage through the entire length of the shell and tube were used (Tab. 1). These times were calculated for both sides separately. Within this load step, the boundary conditions were changed linearly from initial to steady from HTRI using a ramped option.

$$t = \frac{L\rho A}{Q} \tag{1}$$

**Table 1.** Velocity lag in shell/tube duct.

| Duct | Velocity lag in the duct [s] |
|---|---|
| Shell | 1.68 |
| Tube | 1.45 |

Eq. (1) is well applicable for the water duct. In the case of steam duct, it is more difficult to make a prediction because the density and velocity change when steam passes through the shell. For the time the steam passes through the shell, density and mass flow rate for the pure steam ($T$ = 360 °C, $Q$ = 0.025 $kg\,s^{-1}$) were applied.

During the second time step, heat transfer coefficient and bulk temperature field from HTRI steady-state calculation were used. The set-up of time steps and boundary condition is shown in Tabs. 2 and 3 for shell and tubes, respectively. Used surfaces for application of heat transfer coefficient of shell/tubes are also shown in Fig. 4. The end of the second time step was set to 50 s, when the material temperature of shell/tube is practically steady.

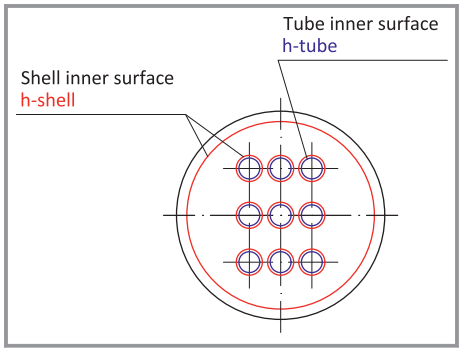


**Figure 4.** Heat transfer coefficient on the shell/tube surfaces.

In this calculation, a simplification as well as the calculation of temperature field and heat transfer coefficient were used. An axisymmetric model was used for shell/tubes. Moreover, the tube bundle was replaced by only one tube.

  

**Table 2.** Set-up of load steps and boundary condition for shell.

| Load step | Time at the end of load step [s] | Bulk temperature depending on the shell length [°C] | | Heat transfer coefficient depending on the shell length [W m$^{-2}$K$^{-1}$] | |
|---|---|---|---|---|---|
| | | Inner surface | Outer surface | Inner face | Outer surface |
| 0 | 1 | 20 | 20 | 20 | 20 |
| 1 | 2.68 | (98.47, 98.47, 82.04, 26.86) | 20 | (8101.9, 24261.0, 1814.5, 984.29) | 20 |
| 2 | 50 | (98.47, 98.47, 82.04, 26.86) | 20 | (8101.9, 24261.0, 1814.5, 984.29) | 20 |

**Table 3.** Set-up of load steps and boundary condition for tubes.

| Load step | Time at the end of load step [s] | Bulk temperature depending on the tube length [°C] | | Heat transfer coefficient depending on the tube length [W m$^{-2}$K$^{-1}$] | |
|---|---|---|---|---|---|
| | | Inner surface | Outer surface | Inner surface | Outer surface |
| 0 | 1 | 20 | 20 | 20 | 20 |
| 1 | 2.45 | (20.51, 20.24, 20.05, 20.0) | (98.47, 98.47, 82.04, 26.86) | (6804.3, 6781.4, 6262.6, 6080.8) | (8101.9, 24261.0, 1814.5, 984.29) |
| 2 | 50 | (20.51, 20.24, 20.05, 20.0) | (98.47, 98.47, 82.04, 26.86) | (6804.3, 6781.4, 6262.6, 6080.8) | (8101.9, 24261.0, 1814.5, 984.29) |

However, in view of 1D results of heat transfer coefficient and bulk temperature field from HTRI used for calculation in this article, it is dispensable to perform full 3D analyses of the tube bundle. The shell/tube model is meshed by axisymmetric PLANE77 elements. The rectangular domain had 500 elements across the length and four elements through the thickness of the shell/tube (2000 on domain). The thermal conductivity of the material for FEM analyses was set at 50 W m$^{-1}$K$^{-1}$, the specific heat was set at 450 J kg$^{-1}$K$^{-1}$.

Fig. 5 shows the material temperature field relative to the length from the midline of the shell (Fig. 5a) and tube (Fig. 5b), respectively, at calculated substeps. The shell material temperature in the steam inlet area rises quickly from 20 to 98 °C in the area of the hot steam inlet. The material temperature of the tubes at the tube inlet area is almost constant in every substep. It rose from 20 to 24.5 °C over time. As expected, the temperature of the tube material rose significantly in the area of intense condensation.

The material temperature field of shell and tubes in every substep is used as an input parameter for the calculation of thermal stress during the start-up process.

## 2.3 Calculation of Thermal Stresses on Shell and Tube Bundle

The axial stress on shell and tubes is investigated. In this calculation, the condenser was simplified to two beams with a fixed support on one side and a coupled axial displace-

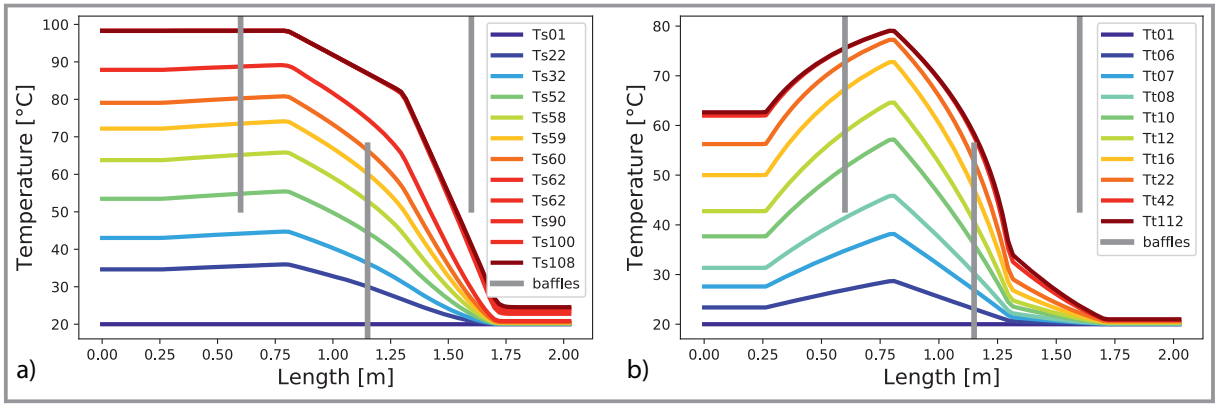


**Figure 5.** Material temperature relative to length of shell/tube in chosen substeps: a) shell, b) tubes.

  

ment on the other side, which represent the shell and the tube bundle (Fig. 6).

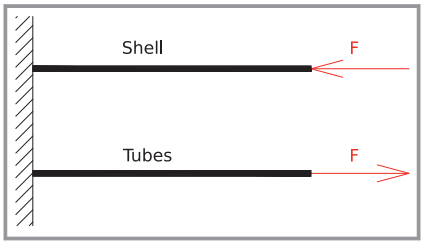


**Figure 6.** Simplified model of shell and tube.

The key step is to collect data on material properties, such as Young's modulus and coefficient of thermal expansion, which are needed to calculate the force which acts on the shell and tubes. For this calculation, polynomial equations (Eqs. (2) and (3)) from the EN 13445 standard, annex O were used.

$$\alpha = c_{\alpha 0} + c_{\alpha 1} T + c_{\alpha 2} T^2 \tag{2}$$

$$E = c_{E0} + c_{E1} T + c_{E2} T^2 \tag{3}$$

The coefficients $c_0$, $c_1$, and $c_2$ are given for material groups according to EN 13445. In the case of the investigated condenser, the shell material is 1.5415 and the tube material is 1.4541. According to the EN 13445 standard, the material group of shell is 1.2 and the material group of tubes is 8.1. The coefficients for polynomial equations are defined in Tab. 4.

It is possible to calculate an axial force equilibrium in accordance with Fig. 5 as shown in Eq. (4). The assumption is that the displacements at the end of the bars are equal:

$$u_S = u_T \rightarrow \alpha_S L_S \Delta T_S - F\frac{L_S}{A_S E_S} = \alpha_T L_T \Delta T_T + F\frac{L_T}{A_T E_T} \tag{4}$$

From Eq. (4), it is possible to evaluate the force equation:

$$F = \frac{\alpha_S L_S \Delta T_S - \alpha_T L_T \Delta T_T}{\frac{L_S}{A_S E_S} + \frac{L_T}{A_T E_T}} \tag{5}$$

Eq. (5) requires a constant value of temperature. Therefore, the course of temperature of the material of shell/tubes was divided into small linear parts which can be described using the linear temperature function equation (Eq. (6)). The temperature differences $\Delta T_S$ and $\Delta T_T$ are related to the temperature before the start-up process, i.e., 20 °C.

$$T = ax + b \tag{6}$$

Because of the calculation of axial displacement on the small linear parts, it is necessary to use the integral calculation of temperature and stiffness in Eq. (5); the displacement is on the linear part, not on the end points.

Using the temperature equation Eq. (6), and Eqs. (2) and (3) for Young's modulus and coefficient of thermal expansion, respectively, it is possible to write Eqs. (7) and (8):

$$\alpha_{S,i}\Delta T_{S,i} = \int_0^{L_{S,i}} \left( \begin{pmatrix} c_{\alpha S0} + c_{\alpha S1}\left(a_{S,i}x_{S,i} + b_{S,i}\right) \\ + c_{\alpha S2}\left(a_{S,i}x_{S,i} + b_{S,i}\right)^2 \end{pmatrix} \left(a_{S,i}x_{S,i} + b_{S,i}\right) \right) \mathrm{d}x_{S,i} \tag{7}$$

$$E_{S,i} = \int_0^{L_{S,i}} \left( c_{ES0} + c_{ES1}\left(a_{S,i}x_{S,i} + b_{S,i}\right) + c_{ES2}\left(a_{S,i}x_{S,i} + b_{S,i}\right)^2 \right) \mathrm{d}x_{S,i} \tag{8}$$

The analog applies to tubes.

Then, it is possible to calculate the axial force (Eq. (9)) necessary to obtain the stresses in the axial direction on the shell and tube bundle, Eqs. (10) and (11):

$$F = \frac{\sum_{i=1}^{n_T} L_{T,i}\alpha\Delta T_{T,i} - \sum_{i=1}^{n_s} L_{S,i}\alpha\Delta T_{S,i}}{\frac{\sum_{i=1}^{n_s} \frac{L_{S,i}}{E_{S,i}}}{A_S} + \frac{\sum_{i=1}^{n_T} \frac{L_{T,i}}{E_{T,i}}}{A_T}} \tag{9}$$

$$\sigma_S = \frac{F}{A_S} \tag{10}$$

$$\sigma_T = \frac{F}{A_T} \tag{11}$$

**Table 4.** Coefficients for polynomial equations for thermal expansion and Young's modulus calculation.

| Coefficient | $c_0$ | $c_1$ | $c_2$ |
|---|---|---|---|
| *Shell* | | | |
| Coefficient of thermal expansion [$K^{-1}$] | $10.98 \cdot 10^{-6}$ | $1.623 \cdot 10^{-8}$ | $-1.287 \cdot 10^{-11}$ |
| Young's modulus [MPa] | $213.16 \cdot 10^{3}$ | −69.1 | $-1.824 \cdot 10^{-2}$ |
| *Tubes* | | | |
| Coefficient of thermal expansion [$K^{-1}$] | $14.97 \cdot 10^{-6}$ | $1.599 \cdot 10^{-8}$ | $-9.990 \cdot 10^{-12}$ |
| Young's modulus [MPa] | $201.66 \cdot 10^{3}$ | −84.8 | 0 |

Fig. 7 shows the stress courses during the start-up process (solid line for shell and dashed line for tubes) and the steady-state stress acting on the shell (dash-dot line) and tubes (dotted line). It is shown that, after the beginning of the start-up process, stress rapidly changes from 0 to around −20 MPa in the case of the tube and from 0 to around 60 MPa in the case of the shell. Therefore, simulation of the start-up process

  

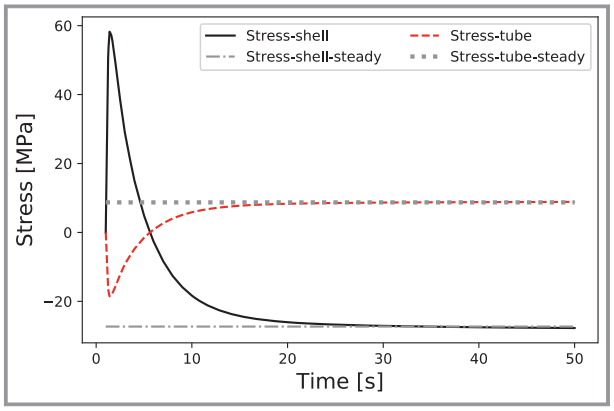


**Figure 7.** Transient thermal stress on shell and tube during the start-up process.

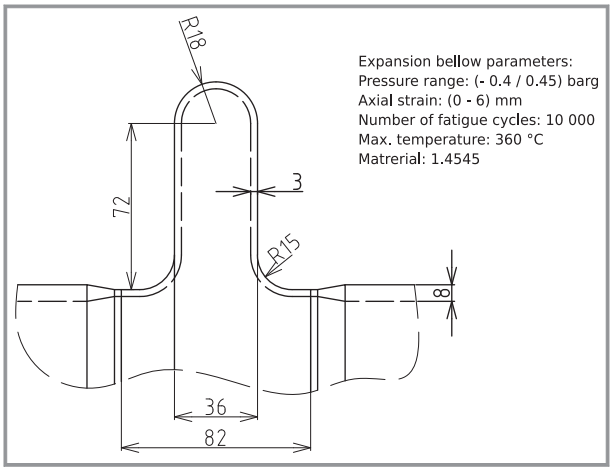


**Figure 8.** Expansion joint geometry.

is absolutely crucial to estimate the thermal stresses in this case because considering only the steady state may lead to underestimation of the stresses and, potentially, an unsafe design.

According to EN 13445, the expansion joint should be used. Therefore, the condenser start-up process with expansion joint was calculated. The expansion joint was designed in advance, so the known geometry was used (Fig. 8). Fig. 9a shows the stress course during the start-up process with and without expansion joint. The thermal longitudinal stress with expansion joint is almost 0 MPa. Exact values of longitudinal stress with expansion joint over time are shown in Fig. 9b, (shell, dashed line; tubes, dotted line). This calculation is also simplified. The geometry of the condenser was replaced by a beam with stiffness of the expansion joint calculated according to EN 13445. Then, the calculation was the same as in the case of a condenser without expansion joint.

The pressure in shell and tubes is not involved in this calculation. Pressure that acts on the tube sheet can have a significant impact on the expansion joint displacement. Moreover, if the start-up and shut-down processes are frequent, expansion joint fatigue could occur. This is one of the reasons why this calculation was made; it is possible to investigate how stiff the expansion joint should be and when it is needed.

## 3 Conclusion

The analysis of the start-up process of a shell and tube condenser is presented in this article. First, the thermal-hydraulic rating is dealt with. The main result from thermal-hydraulic rating is a heat transfer coefficient used for the calculation of shell and tube longitudinal stress. For thermal-hydraulic rating as well as for stress calculation, simplifications were used. The results show how large the stress on the shell and tube bundle during the start-up process should be. Fig. 7 shows that the maximum stress difference is not in the steady state but shortly after the start-up of the condenser. As mentioned, this condenser is a safety type, so frequent start-up and shut-down processes could be expected during the design of this condenser. Frequent start-up and shut-down processes could also lead to fatigue,

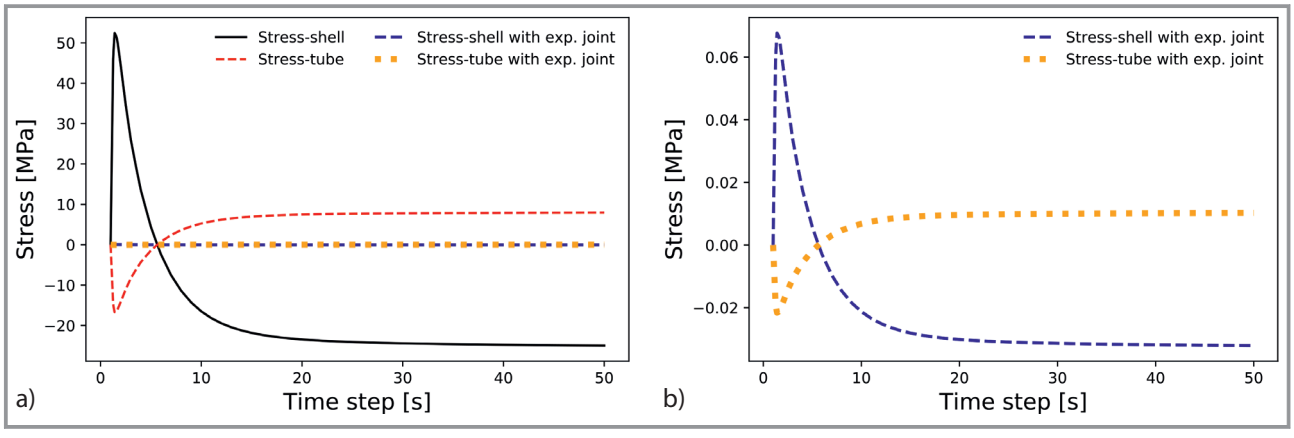


**Figure 9.** Transient thermal stress on shell and tube during the start-up process: a) comparing stress with and without expansion joint, b) longitudinal stress with expansion joint.

  

mainly in the region where the shell and tubes are connected to the tube sheet. This phenomenon could cause a condenser damage leading to a decreased safety of operation.

The calculation of the investigated condenser with expansion joint was also the subject of this article. It was calculated that the thermal stress during the start-up process with expansion joint is around 0 MPa, but the pressure in the shell/tube side is not considered. The shell/tube side pressure can have a high impact on the expansion joint. It could cause failure or even safety problems. Therefore, the future research should be to calculate the thermal stress on the condenser with acting of inside pressure in the shell/tube side. The future research should eliminate some simplifications, mainly as to calculations of the temperature field in transient regime.

The authors gratefully acknowledge the financial support provided by the EU project Strategic Partnership for Environmental Technologies and Energy Production (SPETEP), funded as project No. CZ.02.1.01/0.0/0.0/16_026/0008413 by the Czech Republic Operational Program Research, Development, and Education, Priority Axis 1: Strengthening capacity for high-quality research. The authors also gratefully acknowledge the support provided by the Augsburg University of Applied Sciences. Open access funding enabled and organized by Projekt DEAL.

## Symbols used

| | | |
|---|---|---|
| $A$ | [mm$^2$] | area of duct |
| $a$, $b$ | [–] | linear function coefficient |
| $A_S$ | [mm$^2$] | shell duct area |
| $A_T$ | [mm$^2$] | tube duct area |
| $c_{E0}$, $c_{E1}$, $c_{E2}$ | [MPa] | coefficients for polynomial calculation of Young's modulus |
| $c_{\alpha 0}$, $c_{\alpha 1}$, $c_{\alpha 2}$ | [K$^{-1}$] | coefficients for polynomial calculation of thermal expansion coefficient |
| $E_S$ | [MPa] | Young's modulus for shell |
| $E_T$ | [MPa] | Young's modulus for tubes |
| $F$ | [N] | axial force of shell and tubes |
| *h-shell* | [W m$^{-2}$K$^{-1}$] | heat transfer coefficient of shell |
| *h-tube* | [W m$^{-2}$K$^{-1}$] | heat transfer coefficient of tube |
| $L$ | [mm] | length of duct |
| $L_S$ | [mm] | length of shell |
| $L_T$ | [mm] | length of tube |
| $Q$ | [kg s$^{-1}$] | mass flow rate |
| $t$ | [s] | time |
| $T$ | [°C] | temperature |
| $\Delta T_S$ | [°C] | temperature difference on shell |
| $\Delta T_T$ | [°C] | temperature difference on tube |
| $u_S$ | [mm] | axial displacement of shell |
| $u_T$ | [mm] | axial displacement of tube |

## Greek letters

| | | |
|---|---|---|
| $\alpha_S$ | [K$^{-1}$] | coefficient of thermal expansion of shell |
| $\alpha_T$ | [K$^{-1}$] | coefficient of thermal expansion of tube |
| $\rho$ | [kg m$^{-3}$] | density of process media |
| $\sigma_S$ | [MPa] | thermal stress on shell |
| $\sigma_T$ | [MPa] | thermal stress on tubes |

## Sub- and superscripts

| | |
|---|---|
| E0, E1, E2 | Young's modulus |
| i | time step |
| S | shell |
| T | tube |
| $\alpha 0$, $\alpha 1$, $\alpha 2$ | thermal expansion coefficient |

## Abbreviations

| | |
|---|---|
| CFD | computational fluid dynamics |
| Coef. | coefficient |
| FEM | finite element method |
| HRSG | heat recovery steam generator |

## References

[1] W. Nusselt, *Z. Ver. Dtsch. Ing.* **1916**, *60*, 541–546.
[2] D. Q. Kern, *AIChE J.* **1958**, *4 (2)*, 157–160. DOI: https://doi.org/10.1002/aic.690040208
[3] H. Honda, T. Fujii, B. Uchima, S. Nozu, H. Nakata, *Heat Transfer – Jpn. Res.* **1989**, *18 (6)*, 31–52.
[4] A. Cavallini, D. D. Col, L. Doretti, M. Matkovic, L. Rossetto, C. Zilio, G. Censi, *Heat Transfer Eng.* **2006**, *27 (8)*, 31–38. DOI: https://doi.org/10.1080/01457630600793970
[5] T. Fujii, K. Oda, *Trans. Jpn. Soc. Mech. Eng., B* **1986**, *52 (474)*, 822–826. DOI: https://doi.org/10.1299/kikaib.52.822
[6] A. Cavallini, G. Censi, D. Del Col, L. Doretti, G. A. Longo, L. Rossetto, C. Zilio, *Int. J. Refrig.* **2003**, *26 (4)*, 373–392. DOI: https://doi.org/10.1016/S0140-7007(02)00150-0
[7] M. W. Browne, P. K. Bansal, *Appl. Therm. Eng.* **1999**, *19 (6)*, 565–594. DOI: https://doi.org/10.1016/S1359-4311(98)00055-6
[8] T. Karlsson, L. Vamling, *Int. J. Refrig.* **2005**, *28 (5)*, 706–713. DOI: https://doi.org/10.1016/j.ijrefrig.2004.12.008
[9] X. Wang, N. Zheng, Z. Liu, W. Liu, *Int. J. Heat Mass Transfer* **2018**, *124*, 247–259. DOI: https://doi.org/10.1016/j.ijheatmasstransfer.2018.03.081
[10] J. Wajs, D. Mikielewicz, B. Jakubowska, *Energy* **2018**, *157*, 853–861. DOI: https://doi.org/10.1016/j.energy.2018.05.174
[11] R. Llopis, R. Cabello, E. Torrella, *Int. J. Therm. Sci.* **2008**, *47 (7)*, 926–934. DOI: https://doi.org/10.1016/j.ijthermalsci.2007.06.021
[12] F. Zaversky, M. Sánchez, D. Astrain, *Energy* **2014**, *65*, 647–664. DOI: https://doi.org/10.1016/j.energy.2013.11.070
[13] E. S. Gaddis, E. U. Schlünder, *Verfahrenstechnik* **1975**, *9 (12)*, 617–621./JCIT>
[14] E. S. Gaddis, E. U. Schlünder, *Heat Transfer Eng.* **1979**, *1 (1)*, 43–52. DOI: https://doi.org/10.1080/01457637908939548

  

[15] *HTRI Xchanger Suite User's Guide*, Version 8.0.1, Heat Transfer Research, Inc., Navasota, TX **2019**.
[16] *CHEMCAD*, Chemstations, Inc., Houston, TX **2016**.
[17] *Aspen Exchanger Design and Rating*, Aspen Technology, Inc., Bedford, MA.
[18] J. Taler, P. Dzierwa, M. Jaremkiewicz, D. Taler, K. Kaczmarski, M. Trojan, T. Sobota, *Energy* **2019**, *175*, 645–666. DOI: https://doi.org/10.1016/j.energy.2019.03.087
[19] T. S. Kim, D. K. Lee, S. T. Ro, *Appl. Therm. Eng.* **2000**, *20 (11)*, 977–992. DOI: https://doi.org/10.1016/S1359-4311(99)00081-2
[20] J. Taler, W. Zima, M. Jaremkiewicz, *J. Therm. Stresses* **2016**, *39 (4)*, 386–397. DOI: https://doi.org/10.1080/01495739.2016.1152109
[21] BS EN 13445, *Unfired Pressure Vessels: Requirements for the Design and Fabrication of Pressure Vessels and Pressure Parts Constructed from Spheroidal Graphite Cast Iron*, The British Standards Institution, London **2012**.
[22] *Standards of the Tubular Exchanger Manufacturers Association*, Tubular Exchanger Manufacturers Association, Inc., Tarrytown, NY **2007**.
[23] *ANSYS*, Ansys, Inc., Canonsburg, PA **2019**.

  